ELSEVIER

Available online at www.sciencedirect.com

SCIENCE DIRECT®

Palaeogeography, Palaeoclimatology, Palaeoecology 224 (2005) 311–332

PALAEO

www.elsevier.com/locate/palaeo

Late Pleistocene–Holocene radiolarian paleotemperatures in the Norwegian Sea based on artificial neural networks

Giuseppe Cortese[a,*], Jane K. Dolven[b], Kjell R. Bjørklund[b], Björn A. Malmgren[c]

[a]*Alfred Wegener Institute for Polar and Marine Research (AWI), Columbusstrasse, P.O. Box 120161-27515 Bremerhaven, Germany*
[b]*Geological Museum, University of Oslo, P.O. Box 1172 Blindern, 0318 Oslo, Norway*
[c]*Department of Earth Sciences-Marine Geology, Göteborg University, Box 460, SE-405 30 Göteborg, Sweden*

Received 19 May 2004; received in revised form 13 April 2005; accepted 14 April 2005

Abstract

Artificial Neural Networks (ANN) were trained by using an extensive radiolarian census dataset from the Nordic (Greenland, Norwegian, and Iceland) Seas. The regressions between observed and predicted Summer Sea Temperature (SST) indicate that lower error margins and better correlation coefficients are obtained for 100 m (SST_{100}) compared to 10 m (SST_{10}) water depth, and by using a subset of species instead of all species. The trained ANNs were subsequently applied to radiolarian data from two Norwegian Sea cores, HM 79-4 and MD95-2011, for reconstructions of SSTs through the last 15,000 years. The reconstructed SST is quite high during the Bølling–Allerød, when it reaches values only found later during the warmest phase of the Holocene. The climatic transitions in and out of the Younger Dryas are very rapid and involve a change in SST_{100} of 6.2 and 6.8 °C, taking place over 440 and 140 years, respectively. SST_{100} remains at a maximum during the early Holocene, and this Radiolarian Holocene Optimum Temperature Interval (RHOTI) predates the commonly recognized middle Holocene Climatic Optimum (HCO). During the 8.2 ka event, SST_{100} decreases by ca. 3 °C, and this episode marks the establishment of a cooling trend, roughly spanning the middle Holocene (until ca. 4.2 ka). Successively, since then and through the late Holocene, SST_{100} follows instead a statistically significant warming trend. The general patterns of the reconstructed SSTs agree quite well with previously obtained results based on application of Imbrie and Kipp Transfer Functions (IKTF) to the same two cores for SST_0. A statistically significant cyclic component of our SST record (period of 278 years) has been recognized. This is close to the de Vries or Suess cycle, linked to solar variability, and documented in a variety of other high-resolution Holocene records.

Keywords: Artificial neural networks; Radiolarians; Nordic seas; Late Pleistocene; Holocene

1. Introduction

The Nordic Seas, together with the Labrador Sea, represent today the main site of convection for the deep waters alimenting the North Atlantic Deep

* Corresponding author. Tel.: +49 471 4831 1207; fax: +49 471 4831 1149.
E-mail address: gcortese@awi-bremerhaven.de (G. Cortese).

0031-0182/$ - see front matter © 2005 Elsevier B.V. All rights reserved.
doi:10.1016/j.palaeo.2005.04.015

Water, i.e. the deep return flow of the large-scale overturning circulation. The environmental variables and processes linked to deep-water formation in this area (temperature, salinity and density characteristics of the incoming surface waters, heat release to the atmosphere, sea-ice extent, brine formation) exert a direct control on regional and hemispheric climate. In fact, the thermohaline overturning circulation regulates the heat balance at these high northern latitudes, and during past climate cycles it has shown different equilibrium states (Ganopolski and Rahmstorf, 2001). As these have a direct impact on the climate of surrounding landmasses, it is of interest to reconstruct the changes in the temperature of the main surface water body (i.e. the Norwegian Current) in this climatically sensible area over the Late Pleistocene–Holocene interval, including the last deglaciation.

A broad range of different statistical methods has been used, during the past few decades, to reconstruct paleoclimate. They range from Imbrie and Kipp Transfer Functions (IKTF) (Imbrie and Kipp, 1971) to Canonical Correspondence Analysis (ter Braak, 1986), Modern Analog Technique (MAT) (Hutson, 1979), modern analog with similarity index method (SIMMAX) (Pflaumann et al., 1996), the Revised Analog Method (RAM) (Waelbroeck et al., 1998), Weighted Averaging Partial Least Squares (WA-PLS) (ter Braak and Juggins, 1993; Birks, 1995), and Artificial Neural Networks (ANN) (McCulloch and Pitts, 1943; Malmgren and Nordlund, 1997).

Several of these techniques were successfully used to extract paleoclimatic information from census data based on different microfossil groups. IKTF has been applied to radiolarians from the Pacific Ocean (Moore, 1973; Molina-Cruz, 1984; Pisias et al., 1997), the Southern Ocean (Abelmann et al., 1999; Cortese and Abelmann, 2002), the Atlantic Ocean (Morley, 1979), and the Nordic Seas (Bjørklund et al., 1998; Dolven et al., 2002; Cortese et al., 2003). In this paper, ANNs were trained on the basis of radiolarian relative abundance data from surface sediment samples collected in the Nordic Seas, and the trained ANNs were applied to high-resolution down-core records from the eastern Norwegian Sea (cores HM79-4 and MD95-2011). We will present the main results obtained from the network calibration phase, and the obtained SST_{100} (Summer Sea Temperature at 100 m) estimates. The down-core paleotemperature predictions based on ANN will be discussed in relation to other Late Pleistocene–Holocene paleoclimatic records.

2. Methods

2.1. "*Artificial*" neural networks and statistical testing procedures

Artificial Neural Networks (ANN) are "self-adjusting" computer systems that can "learn" by continuously going back and changing a set of parameters in the model to reduce the error between a desired output and an actual output, i.e. in our case finding the optimal model for reconstructing SST_{100} from a given dataset. Our ANNs were trained on the basis of radiolarian census data collected from 161 surface sediment samples (Fig. 1, inset) from the Nordic Seas (Cortese et al., 2003). In order to reconstruct paleotemperatures, the ANNs were then applied to down-core radiolarian census data from two cores, HM79-4 and MD95-2011 (Dolven et al., 2002), sampled in the eastern Norwegian Sea (Fig. 1). Two different ANN programs, the NeuroGenetic Optimizer (NGO, version 2.5; ©BioComp Systems, Inc.) and the iModel (version 1.5, ©BioComp Systems, Inc.), were initially used to assess which of them worked best. We found, based on three test runs, that the NGO generated slightly lower error rates than the iModel, so we used the NGO software in the ensuing analyses. We used the Root-Mean-Square Error of Prediction (RMSEP), which is the square root of the sum of the squared differences between the observed and predicted values for all observations in the test set divided by the number of such observations, to estimate the prediction error. We also made three separate training runs for 10 and 100 m water depth using the NGO, in order to assess the lowest RMSEP (Table 1), and found that the reconstruction of temperatures at 100 m provides best results (average RMSEP = 0.77; average $r = 0.96$).

In our analyses, the original data were automatically subdivided by the software into a training and a test set using a random procedure. For the 161 surface sediment samples included in the dataset, 120 samples were used as the modelling/training set, and the

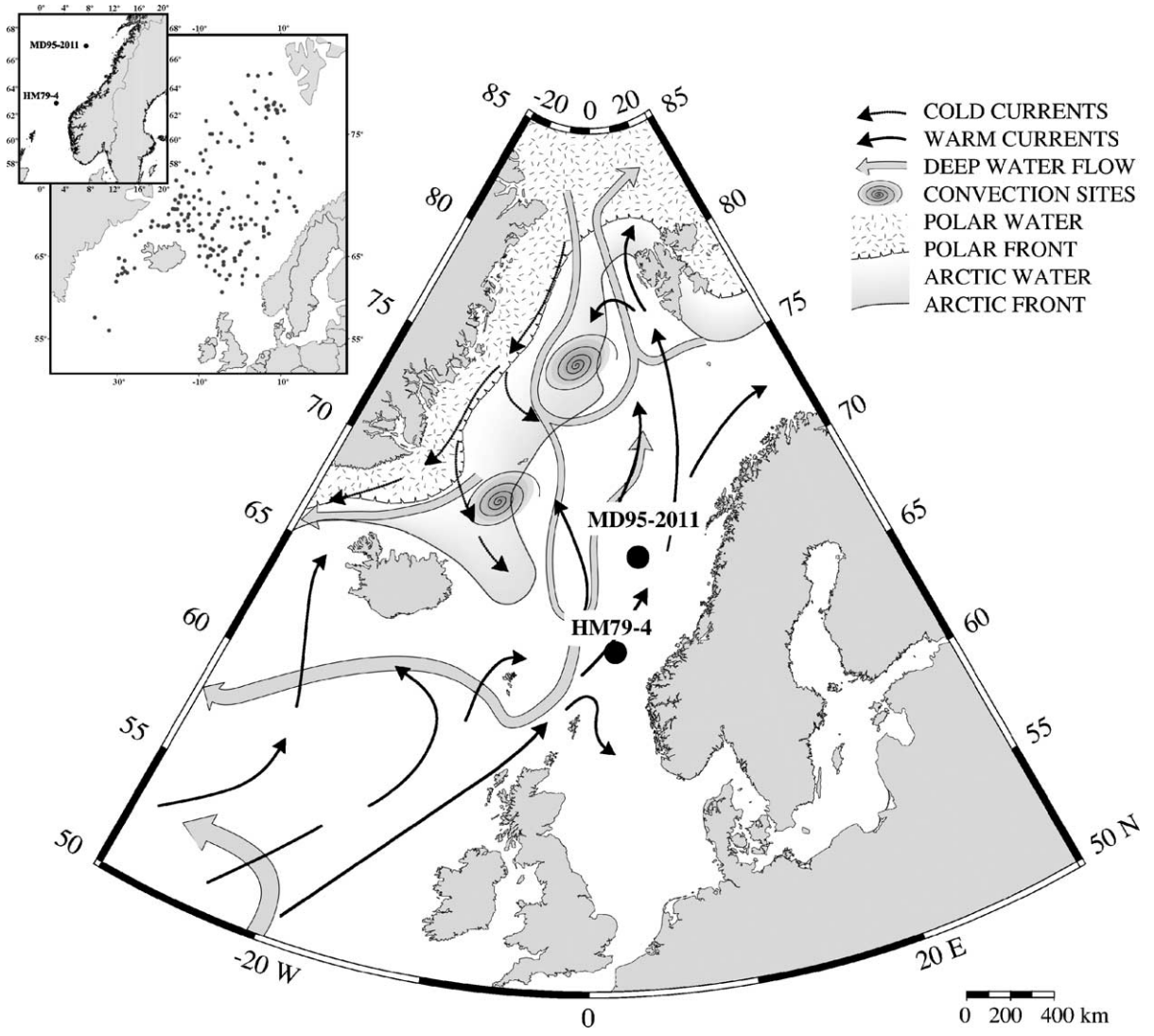

Fig. 1. Location map, modified after Risebrobakken et al. (2003). The position of the studied cores is shown: HM79-4 (63°06′ N, 02°33′ E) and MD95-2011 (66°58′ N, 07°38′ E). The main surface and deep currents, as well as other important oceanographic features (Polar and Arctic Front, deep-water convection sites) are reported too. The inset displays the 161 surface sediment samples used for the calibration to modern hydrography conditions (Cortese et al., 2003).

remaining 41 samples as the test set. As the randomly picked test-set samples are not included in the training process, the error rates are based on this set. They therefore provide estimates of the prediction error rate in samples different than those used in the training set. In other words, the RMSEP represents an estimate of the minimum error we can expect when using the trained ANNs to "predict" past SSTs. Obtaining an RMSEP of 1.0, if the estimated SST is 7 °C, means that the estimated error in paleo-SSTs predictions is at least 1 °C, i.e. 7 ± 1 °C. In this sense, low RMSEP are equivalent to being able to generate past SSTs with a low error.

In tests for trend in timeseries, the confidence interval for the slope coefficient of the regression function can only be used in cases where the sequence of residuals is random and independent (uncorrelated), with residuals conforming to the normal

Table 1
Summary of NGO training runs

NGO all species			NGO subset		
	RMSEP	*r*		RMSEP	*r*
10 m					
Run 1	1.3861	0.8751	Run 1	1.1597	0.9148
Run 2	1.2048	0.9316	Run 2	0.9978	0.9422
Run 3	1.2753	0.9064	Run 3	1.0484	0.9384
Mean	1.2887	0.9044		1.0686	0.9318
100 m					
Run 1	0.9485	0.9329	Run 1	0.8619	0.9477
Run 2	0.8352	0.9566	Run 2	0.7222	0.967
Run 3	0.7795	0.9607	Run 3	0.7321	0.9654
Mean	0.8544	0.9501		0.7721	0.96

Root Mean Square Error of Prediction (RMSEP) and correlation coefficient between observed and estimated SST (r), along with their mean values, are shown for three different runs.

distribution. Since all of these assumptions were not met here, the Kendall test (Kendall and Ord, 1990) was used instead. We employed the REDFIT procedure, introduced by Schulz and Mudelsee (2002), to test for cyclical patterns in the generated SST_{100} timeseries. REDFIT is specifically adapted to unevenly spaced timeseries, and allows tests of the significance of peaks in the spectrum against a null-hypothesis of a red-noise background, which is estimated using an AR1 process. The REDFIT technique avoids the significant bias in the form of reddening of the spectrum that results from interpolations in the time domain to artificially create equal sampling intervals. The REDFIT procedure is associated with a runs test, aimed at assessing whether the spectrum is consistent or not with a red-noise model. If the r-value resulting from this test lies within a 5% acceptance region, an AR1 model is appropriate to characterize the record. We used a false-alarm level of $(1-1/n)*100\%$, where n is the number of spectral values in the timeseries (Thomson, 1990), which is the maximum spectral amplitude expected if the timeseries were generated by an AR1 process (Schulz and Mudelsee, 2002), as the lower level for the detection of non-AR1 components in the timeseries. In our application, the false-alarm level is 98.4%. We used the mean of 2000 Monte Carlo simulations of the AR1 process to estimate the red-noise spectra in our applications (the over-sampling factor for the Lomb–Scargle Fourier transform was set at 3.0 and the number of Welch-overlapped-segments with 50% overlap at 3, and we used a Welch spectral window to reduce spectral leakage; details on the parameters can be found in Schulz and Mudelsee, 2002).

2.2. Species selection

We also operated a selection of taxa, as the 30 taxa that were included in any further statistical treatment (Table 2, Plates I and II) were chosen from an original species list comprising 114 taxa, most of which were identified to species level. During this screening phase (see Cortese et al., 2003, for additional details), taxa are excluded if they are intermediate/deep water dwellers (e.g. *Cycladophora davisiana*, *Eucyrtidium calvertense*); if taxonomic uncertainties could lead to lumping or wrong identification; if a dissolution bias is present (e.g. species particularly prone/resistant to dissolution). All these reasons blur the value of these taxa as SST reconstruction tools, and therefore lower the correlation coefficients attached to them, and widen the error bars. As our objective was to obtain reliable SST estimates (based on biology/ecology information) from the ANN, and not to optimize error rates, we however preferred to operate the initial species screening (the 30 pre-selected taxa) ourselves and not leave it to an automated routine. The pre-selection gives us the possibility to integrate into the dataset information concerning radiolarian ecology, habitat preferences (e.g. shallow vs. deep water living taxa), deviation from a simple relation to SST (taxa influenced by other environmental parameters), that cannot be assessed independently by ANN, and which will introduce a strong amount of noise to the estimates. This information comes from additional material, previous studies and published literature (Bjørklund et al., 1998; Cortese et al., 2003), and experience that is not reflected and/or included in the dataset. Within the 30 pre-selected taxa (Table 2), we then let the software automatically pick "subsets" of taxa as inputs to the program, and assess which species setup will produce the lowest RMSEPs. This procedure was preferred to manually adding or deleting arbitrarily one or more taxa and then training the networks over and over again, since the ANN procedure is quite time-consuming. With our current setup, each network has to be run for ca. 12 h, and to

Table 2
Artificial Neural Network configuration for the prediction of SST_{100}

	N1	N2	N3	N4	N5	N6	N7	N8	N9	N10
RMSEP	0.759	0.722	0.723	0.768	0.715	0.721	0.740	0.705	0.618	1.003
r	0.959	0.967	0.967	0.957	0.958	0.951	0.958	0.964	0.973	0.917
Species selection										
Actinomma leptoderma/boreale group	X	X	X		X		X	X	X	X
Actinomma leptoderma longispina	X		X	X	X	X		X	X	X
Actinomma medianum				X				X		
Actinomma popofskii		X	X		X	X				
Actinomma sp. 2	X						X	X		
Amphimelissa setosa		X			X	X				X
Artobotrys boreale		X		X		X	X	X	X	
Artostrobus joergenseni				X	X	X			X	
Ceratocyrtis galeus	X	X							X	
Ceratocyrtis histricosus						X				
Corocalyptra craspedota			X	X		X				
Larcospira minor	X		X	X	X	X	X	X	X	X
Larcospira sp. 1	X	X		X		X		X	X	X
Lipmanella xiphephorum	X			X		X				
Lithelius spiralis	X		X				X	X		
Lithomelissa hystrix			X	X	X	X	X		X	
Lithomelissa setosa	X	X	X	X	X	X	X	X	X	X
Lithomelissa sp. aff. *L. stigi*	X	X	X			X	X			
Lithomelissa thoracites	X	X	X	X	X	X	X	X	X	X
Lithomitra lineata	X	X	X	X	X				X	
Phorticium clevei	X	X	X		X	X	X	X	X	X
Phorticium sp. 1		X			X	X		X	X	
Plagiacantha arachnoides		X	X	X	X	X	X		X	
Plectacantha oikiskos	X		X	X		X	X	X	X	
Pseudodictyophimus gracilipes		X		X		X	X	X	X	
Sethoconus tabulatus		X	X	X	X				X	X
Streblacantha circumtexta		X	X	X		X			X	
Streblacantha sp.1			X				X			
Stylatractus sp. 1		X	X	X		X	X		X	X
Tholospyris gephyristes				X	X	X			X	

Root Mean Square Errors of Prediction (RMSEP), correlation coefficients (r) for the relationship between observed and predicted SST in the test sets, and the taxa used are reported for each network configuration.

be able to obtain an accurate estimate of the RMSEP, the same dataset needs to be run several times with different training/test set splits, selected by the program.

2.3. Core sampling and chronology

All radiolarian samples used in this study have been described in previous papers. See: Cortese et al. (2003), for the 161 surface sediment samples (shown in the inset of Fig. 1), and Dolven et al. (2002), for core HM79-4 (63°06′ N, 02°33′ E) and core MD95-2011 (66°58′ N, 07°38′ E). The studied cores were recovered by the R/V Håkon Mosby (during a campaign organized by the Geological Institute, University of Bergen), and by the R/V Marion Dufresne (during IMAGES cruise 101), respectively. A total of 64 samples were collected from a 1.85 m (55.5–240.4 cm) long section of core HM79-4, spanning 9880–13,400 ^{14}C years B.P., with a resulting average sedimentation rate of 52 cm/1000 years, and an average sampling resolution of 55 years. Core MD95-2011 provided 126 samples from a 6.40 m long section (15.5–655.5 cm), dated at 600–9770 ^{14}C years B.P., thus resulting in an average sedimentation rate of 70 cm/1000 years, and an average

sampling resolution of 73 years. Note that the first few hundred years in core MD95-2011 were lost during coring operations.

The Vedde Ash layer (Birks et al., 1996), sixteen AMS ^{14}C-datings of *Neogloboquadrina pachyderma* (Koc-Karpuz and Jansen, 1992), and the peak occur-

Plate I. Spumellarians. All figures, scale bar is 100 μm (see page 317).

1. *Actinomma boreale*, St. V27-94, Norwegian Sea
2. *Actinomma popofskii* Petrushevskaya, 1968 (*Actinomma* sp.1 in Cortese et al., 2003), St. GIK17056, North Atlantic
3. *Actinomma popofskii* Petrushevskaya, 1968 (*Actinomma* sp.1 in Cortese et al., 2003), St. GIK17056, North Atlantic
4. *Actinomma leptoderma longispina*, St. GIK23417, North Atlantic
5. *Actinomma* sp. 2, St. 10, Nærøyfjorden
6. *Actinomma medianum*, St. GIK23417, North Atlantic
7. *Larcospira minor*, St. V27-94, Norwegian Sea
8. *Larcospira minor*, St. V27-94, Norwegian Sea
9. *Actinomma leptoderma longispina*, St. V27-94, Norwegian Sea
10. *Stylatractus* sp. 1, St. GIK17056, North Atlantic
11. *Actinomma leptoderma*, St. V27-94, Norwegian Sea
12. *Lithelius spiralis*, St. V27-94, Norwegian Sea
13. *Phorticium (clevei) pylonium*, St. V27-94, Norwegian Sea
14. *Streblacantha circumtexta*, St. 10, Nærøyfjorden
15. *Phorticium* sp. 1, St. GIK23413, North Atlantic
16. *Larcospira* sp. 1, St. V27-94, Norwegian Sea
17. *Larcospira* sp. 1, St. V27-94, Norwegian Sea
18. *Streblacantha* sp. 1, St. V27-94, Norwegian Sea

Plate II. Nassellarians. 1–8, 11 and 13, scale bar is 50 μm. All other figures, scale bar is 100 μm (see page 318).

1. *Amphimelissa setosa*, St. V27-46, Norwegian Sea
2. *Amphimelissa setosa*, St. V27-94, Norwegian Sea
3. *Artobotrys boreale*, St. V27-94, Norwegian Sea
4. *Artobotrys boreale*, St. V27-94, Norwegian Sea
5. *Artostrobus joergenseni*, St. V27-94, Norwegian Sea
6. *Artostrobus joergenseni,* St. V27-46, Norwegian Sea
7. *Lithomelissa thoracites*, St. V27-94, Norwegian Sea
8. *Lithomelissa setosa*, St. V27-94, Norwegian Sea
9. *Lithomitra lineata*, St. V27-94, Norwegian Sea
10. *Lithomitra lineata*, St. V27-94, Norwegian Sea
11. *Lithomelissa setosa*, St. V27-94, Norwegian Sea
12. *Lithomelissa* sp. aff. *L. stigi*, St. V27-94, Norwegian Sea
13. *Sethoconus tabulatus*, St. V27-94, Norwegian Sea
14. *Plectacantha oikiskos*, St. V27-94, Norwegian Sea
15. *Lithomelissa hystrix*, St. V27-94, Norwegian Sea
16. *Lithomelissa hystrix*, St. V27-94, Norwegian Sea
17. *Pseudodictyophimus gracilipes*, St. V27-94, Norwegian Sea
18. *Pseudodictyophimus gracilipes*, St. V27-94, Norwegian Sea
19. *Lithomelissa* sp. aff. *L. stigi*, St. V27-94, Norwegian Sea
20. *Pseudodictyophimus gracilipes*, St. V27-94, Norwegian Sea
21. *Ceratocyrtis galeus*, St. V23-76, Norwegian Sea
22. *Ceratocyrtis histricosus*, St. V23-76, Norwegian Sea
23. *Tholospyris gephyristes*, St. V27-94, Norwegian Sea
24. *Plagiacantha arachnoides*, St. 25, Balsfjord
25. *Ceratocyrtis galeus*, St. V27-94, Norwegian Sea
26. *Corocalyptra craspedota*, St. V23-76, Norwegian Sea
27. *Corocalyptra craspedota*, St. V23-76, Norwegian Sea
28. *Lipmanella xiphephorum*, St. V23-76, Norwegian Sea

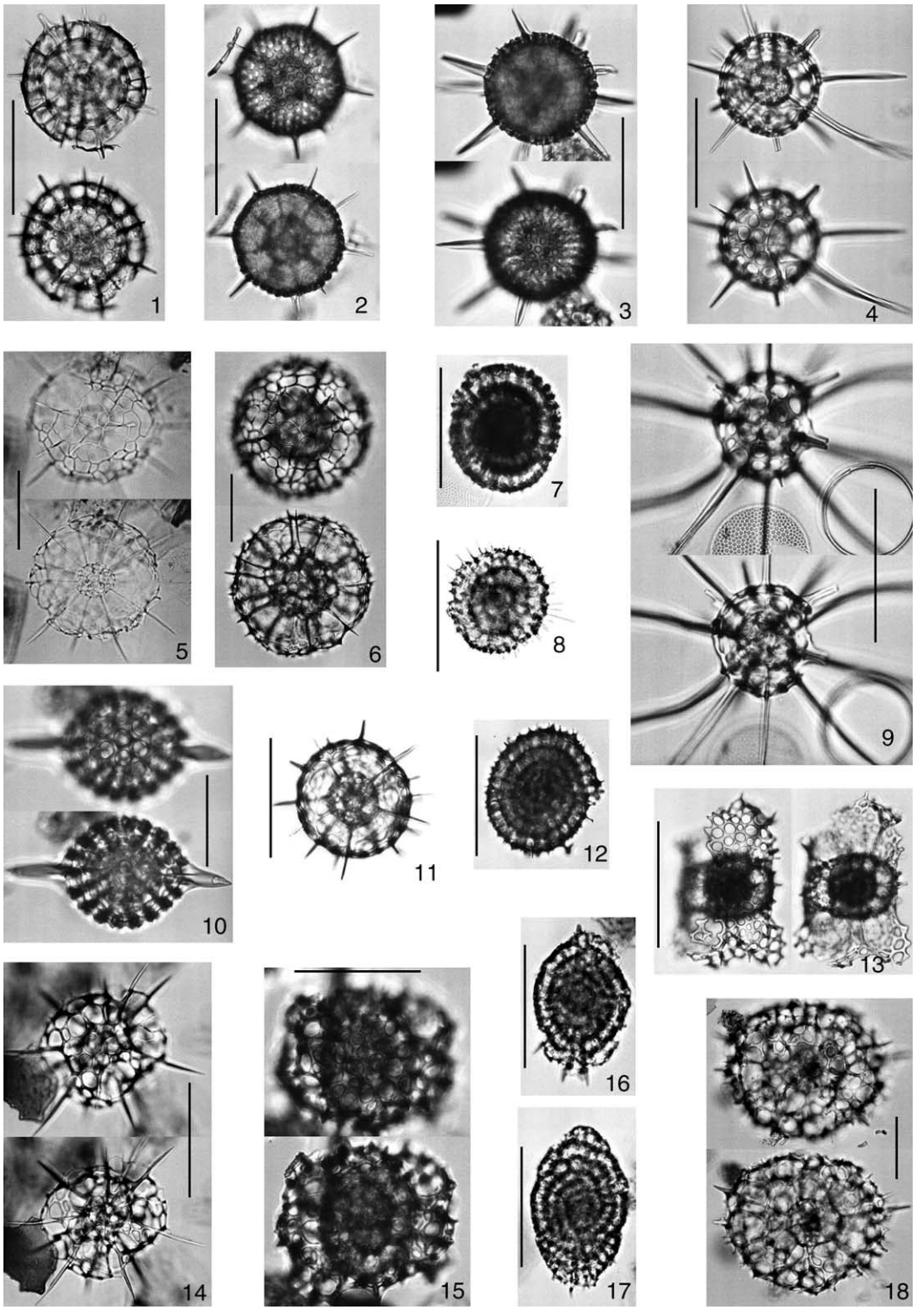

Plate I (*caption on page 316*).

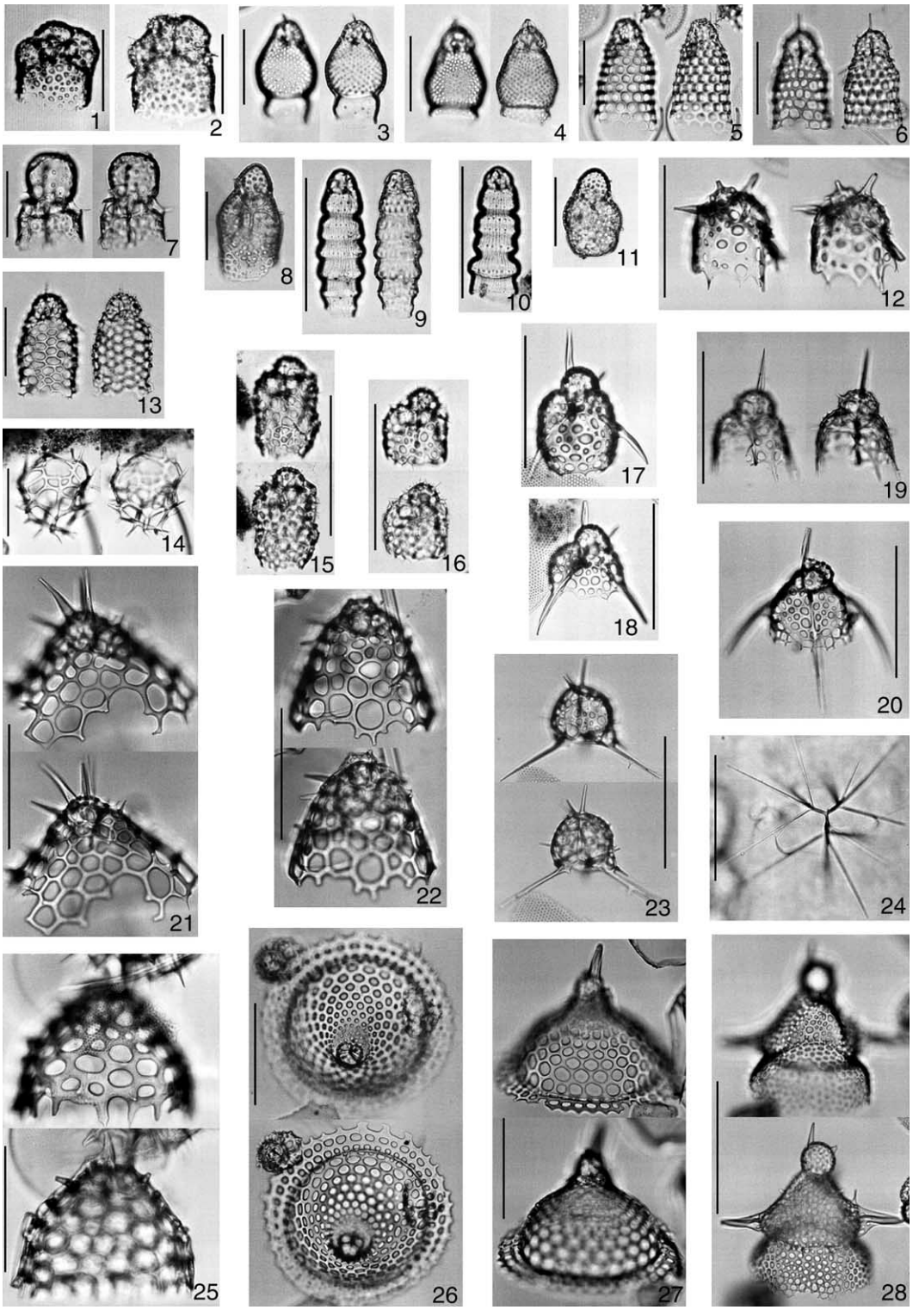

Plate II (*caption on page 316*).

rence of the radiolarian species *Rhizoplegma boreale* (Dolven and Bjørklund, 2001) were used to develop the age model of the two cores and correlate them. The precision of the ^{14}C age determinations for the dating points is better than ± 100 years for the Holocene section, and ca. ± 150 years for the older part. All dating points, as well as the tie points for the synchronization of the calendar year chronology to the GISP ice core, are listed in Dolven et al. (2002). The correction of the previous age model, by peak-to-peak correlation of our SST and the GISP $\delta^{18}O$ records, was necessary to account for the assumingly longer residence time of seawater in the study area during glacial times, which tends to produce artificially older ages during these time intervals. In this paper we have used the calendar year chronology developed from correlation to the GISP ice core (Table 3) when plotting our figures. Further details on sampling, preparation and raw data production, as well as the chronology of the two cores, are available in Dolven et al. (2002) and Cortese et al. (2003).

2.4. Hydrography

We interpolated temperature data for the warm season (Summer Sea Temperature, SST) at the 161 surface sediment sample sites by using the multiplatform oceanography visualization software Ocean Data View (Schlitzer, 2000). This procedure was carried out automatically based on the geographic position of our cores and a regular overlay grid represented by the one degree-spaced World Ocean Atlas data (Conkright et al., 1998). SST represents seasonally averaged July–September (summer) temperatures for 100 m (SST_{100}) depth.

2.5. Seasonality

Regression techniques are often used to estimate both cold- and warm-season temperatures. We however reconstructed only warm-season temperatures, as we believe that the specimens embedded and preserved in the sediment are mainly those produced during spring/summer, when radiolarian peak production takes place. This is in good agreement with studies previously carried out in the Nordic Seas, based on sediment traps and on vertical profiles of both species and specimens abundances (Schröder-

Table 3
Downcore data for cores MD95-2011 and HM79-4: for each sample depth, the IKTF-SST_0 (Dolven et al., 2002) and the ANN-SST_{100} and its 95% confidence interval are reported, along with the age assignment of each sample (in calendar years Before Present), for both the original age model (as shown in Dolven et al., 2002; Table 3), and for the GISP-synchronized age model used in the present paper (see text for details).

Depth (cm)	Calendar age	Age GISP	SST0 IKTF	SST100 ANN	SST100 ANN
MD95-2011	(years BP)	(years BP)	(°C)	(°C)	95% CI (°C)
15.5	567	1001	11.8	7.0	0.2
19.5	581	1013	12.8	6.7	0.4
24.5	600	1030	12.5	6.3	0.5
29.5	618	1046	12.8	6.5	0.3
35.5	641	1066	12.7	6.7	0.3
41.5	663	1085	12.3	6.9	0.2
44.5	674	1095	12.6	6.9	0.2
49.5	711	1127	11.1	5.7	0.7
55.5	788	1184	13.0	6.3	0.3
59.5	839	1221	12.7	6.8	0.2
65.5	917	1279	12.1	4.9	0.4
69.5	968	1316	12.0	6.1	0.5
75.5	1026	1359	11.7	6.1	0.4
81.5	1080	1399	11.6	5.7	0.4
85.5	1116	1426	10.9	4.3	0.7
90.5	1164	1461	11.9	6.9	0.2
95.5	1225	1506	11.1	4.6	0.3
101.5	1298	1560	11.4	4.0	0.4
105.5	1347	1596	12.1	6.6	0.4
109.5	1395	1631	12.0	6.0	0.4
115.5	1468	1685	11.8	5.2	0.6
124.5	1578	1766	11.8	6.0	0.7
129.5	1639	1811	10.5	5.3	0.4
135.5	1712	1897	11.0	4.8	0.4
139.5	1761	1954	12.0	6.4	0.5
145.5	1834	2039	12.4	6.9	0.2
148.5	1870	2082	12.6	6.8	0.3
155.5	1971	2200	11.3	5.1	0.6
160.5	2082	2330	12.0	6.6	0.2
165.5	2194	2461	12.1	6.2	0.3
170.5	2306	2592	12.0	6.6	0.2
175.5	2379	2678	12.3	6.2	0.4
180.5	2452	2763	12.4	6.4	0.4
185.5	2526	2850	12.8	6.6	0.3
190.5	2599	2936	12.5	6.5	0.3
195.5	2672	3021	11.8	4.8	0.5
200.5	2745	3107	12.1	6.3	0.3
205.5	2818	3192	12.1	6.0	0.4
210.5	2891	3278	12.1	5.0	0.4
215.5	2965	3364	12.4	6.3	0.3
219.5	3023	3432	12.5	6.5	0.4
225.5	3111	3536	11.6	4.7	0.6
230.5	3184	3621	11.6	5.1	0.7
235.5	3257	3707	12.4	6.6	0.3

(continued on next page)

Table 3 (*continued*)

Depth (cm)	Calendar age	Age GISP	SST0 IKTF	SST100 ANN	SST100 ANN
MD95-2011	(years BP)	(years BP)	(°C)	(°C)	95% CI (°C)
240.5	3331	3793	12.6	6.5	0.4
245.5	3404	3879	11.6	4.7	0.4
250.5	3477	3964	11.5	5.3	0.4
255.5	3550	4050	12.9	6.6	0.4
260.5	3623	4135	11.3	4.2	0.5
265.5	3696	4221	11.1	3.8	0.6
270.5	3768	4305	11.3	4.9	0.5
275.5	3834	4383	11.4	4.6	0.4
280.5	3900	4460	12.1	6.0	0.3
285.5	3966	4537	12.5	6.2	0.4
289.5	4019	4599	11.5	4.4	0.4
295.5	4099	4693	10.9	4.3	0.4
298.5	4138	4729	11.9	6.0	0.5
306.5	4244	4826	12.8	5.4	0.5
312.5	4323	4899	11.8	5.2	0.4
326.5	4527	5086	12.3	6.5	0.3
329.5	4576	5131	11.8	6.2	0.5
334.5	4657	5205	11.7	5.8	0.4
339.5	4739	5280	11.2	5.4	0.4
344.5	4820	5355	12.0	5.6	0.4
349.5	4902	5430	11.7	5.0	0.3
354.5	4984	5505	12.1	5.8	0.3
359.5	5065	5580	12.5	5.8	0.4
364.5	5147	5655	12.3	6.6	0.3
369.5	5228	5729	11.8	5.7	0.5
374.5	5310	5804	11.3	5.1	0.6
378.5	5375	5864	12.0	6.6	0.3
384.5	5473	5954	11.5	6.5	0.3
389.5	5554	6028	11.5	5.4	0.5
394.5	5636	6104	11.5	5.2	0.3
399.5	5717	6178	12.1	5.6	0.5
404.5	5799	6253	12.5	6.8	0.2
409.5	5881	6329	11.7	5.9	0.4
414.5	5962	6403	12.1	6.3	0.5
419.5	6044	6478	12.4	6.7	0.3
424.5	6125	6553	11.6	5.4	0.3
428.5	6190	6612	11.7	6.3	0.3
434.5	6288	6702	12.0	6.5	0.3
438.5	6354	6763	12.3	6.5	0.2
444.5	6451	6852	11.5	5.3	0.8
448.5	6517	6912	12.0	5.6	0.3
455.5	6631	7017	11.8	6.5	0.3
460.5	6712	7091	11.3	5.5	0.6
465.5	6794	7167	12.3	7.2	0.1
470.5	6876	7242	12.0	6.9	0.2
475.5	6957	7316	11.9	6.9	0.3
480.5	7039	7391	11.5	5.7	0.4
485.5	7120	7466	11.1	6.6	0.3
490.5	7202	7541	10.4	4.7	0.8
495.5	7283	7618	12.0	7.3	0.2
500.5	7365	7696	10.7	4.7	0.7
505.5	7446	7774	11.9	6.7	0.4

Table 3 (*continued*)

Depth (cm)	Calendar age	Age GISP	SST0 IKTF	SST100 ANN	SST100 ANN
MD95-2011	(years BP)	(years BP)	(°C)	(°C)	95% CI (°C)
510.5	7528	7852	12.2	6.9	0.2
515.5	7609	7929	10.7	4.7	0.5
520.5	7691	8007	10.7	5.6	0.4
525.5	7819	8129	10.5	4.9	0.6
530.5	7948	8252	10.4	5.3	0.6
535.5	8076	8400	12.5	7.4	0.2
540.5	8204	8548	11.9	7.6	0.2
545.5	8332	8697	11.6	6.9	0.2
550.5	8461	8846	13.0	7.6	0.2
555.5	8589	8994	12.4	7.2	0.2
560.5	8717	9142	12.0	7.1	0.2
565.5	8846	9292	12.1	7.6	0.2
570.5	8974	9440	12.6	7.2	0.1
575.5	9102	9588	12.0	7.4	0.1
580.5	9231	9737	12.2	7.2	0.1
585.5	9359	9886	12.1	7.2	0.2
590.5	9487	10,034	11.7	7.3	0.2
595.5	9615	10,182	12.4	7.5	0.2
602.5	9795	10,390	12.0	7.4	0.2
605.5	9872	10,480	11.4	6.6	0.3
610.5	10,000	10,628	12.2	7.4	0.1
615.5	10,128	10,776	11.9	7.3	0.2
620.5	10,256	10,924	12.3	7.8	0.2
625.5	10,385	11,074	12.5	7.9	0.3
630.5	10,513	11,222	11.9	7.2	0.2
635.5	10,641	11,370	10.0	6.2	0.5
640.5	10,770	11,407	11.0	7.3	0.1
645.5	10,898	11,444	10.7	6.8	0.3
650.5	11,026	11,480	12.0	7.7	0.2
655.5	11,155	11,517	11.4	6.8	0.3

Depth (cm)	Calendar age	Age GISP	SST0 IKTF	SST100 ANN	SST100 ANN
HM79-4	(years BP)	(years BP)	(°C)	(°C)	95% CI (°C)
55.5	11,155	11,517	10.5	7.5	0.2
60.5	11,275	11,552	9.9	7.0	0.2
65.5	11,394	11,586	8.9	3.1	0.5
70.5	11,514	11,620	7.4	1.3	0.7
75.5	11,633	11,655	7.2	0.7	0.3
80.5	11,753	11,689	7.1	0.8	0.2
84.5	11,849	11,777	7.3	0.9	0.6
86.5	11,896	11,821	7.6	1.5	0.6
91.5	12,066	11,977	7.5	1.6	0.6
95.5	12,297	12,190	7.6	1.1	0.7
100.5	12,584	12,455	8.0	1.2	0.8
103.0	12,728	12,588	7.3	0.8	0.3
105.5	12,872	12,720	7.5	0.8	0.6
108.0	13,016	12,853	7.4	0.8	0.6
110.5	13,146	12,900	8.2	1.8	0.5
113.0	13,218	12,926	8.6	1.6	0.6

Table 3 (*continued*)

Depth (cm)	Calendar age	Age GISP	SST0 IKTF	SST100 ANN	SST100 ANN
HM79-4	(years BP)	(years BP)	(°C)	(°C)	95% CI (°C)
115.5	13,290	12,951	8.4	1.4	0.6
118.0	13,363	12,978	8.3	1.2	0.7
120.5	13,435	13,004	7.6	1.1	0.6
123.5	13,522	13,035	7.6	0.8	0.6
127.5	13,638	13,076	7.8	2.0	0.6
130.5	13,724	13,107	7.6	0.7	0.4
134.0	13,826	13,144	7.4	0.7	0.5
137.0	13,913	13,215	8.3	1.5	0.7
140.5	14,014	13,297	8.5	1.2	0.7
143.0	14,086	13,356	7.9	1.1	0.6
146.5	14,151	13,409	8.5	1.5	0.7
150.0	14,167	13,422	9.6	2.4	0.8
153.0	14,180	13,432	8.3	1.1	0.7
155.5	14,192	13,442	9.4	3.4	0.6
158.0	14,203	13,451	9.5	3.4	0.6
160.5	14,214	13,460	8.6	1.3	0.6
163.0	14,226	13,470	8.5	1.7	0.6
165.5	14,237	13,479	9.4	3.0	0.5
168.0	14,248	13,488	9.3	3.4	0.7
170.5	14,260	13,497	8.5	2.1	0.7
173.0	14,271	13,506	8.0	0.9	0.4
176.5	14,319	13,545	8.2	1.8	0.7
178.5	14,371	13,588	8.9	2.2	0.6
180.5	14,422	13,629	9.2	2.6	0.6
183.0	14,487	13,682	8.2	0.6	0.2
186.5	14,577	13,755	8.9	2.9	0.6
188.5	14,629	13,798	8.8	2.2	0.6
191.5	14,707	13,861	8.9	2.7	0.5
193.0	14,745	13,892	9.3	3.2	1.1
195.5	14,810	13,945	9.0	2.5	0.6
198.0	14,875	13,998	9.1	4.7	0.5
200.5	14,939	14,050	8.7	3.5	0.6
203.0	15,004	14,087	9.9	6.2	0.4
205.5	15,069	14,124	9.6	6.8	0.5
208.0	15,133	14,161	9.6	6.5	0.7
210.5	15,198	14,198	10.3	7.0	0.4
213.0	15,263	14,235	10.1	7.2	0.2
215.5	15,327	14,271	10.1	6.3	0.6
218.0	15,392	14,308	10.3	6.5	0.5
220.5	15,456	14,345	11.1	7.6	0.1
223.0	15,521	14,382	11.0	7.0	0.2
226.5	15,612	14,434	11.5	7.6	0.2
228.0	15,650	14,455	11.6	7.2	0.2
231.5	15,743	14,508	11.6	5.8	0.6
233.0	15,783	14,531	12.1	6.7	0.4
236.5	15,878	14,585	11.3	4.0	0.6
238.5	15,932	14,616	11.4	4.6	0.7
240.5	15,986	14,647	11.6	4.1	0.4

Ritzrau, 1995). This is also supported by plankton studies in Korsfjorden, where the standing stock of living radiolarians reached highest values (individuals/m^3) during the summer (Bjørklund, 1974).

3. Results

3.1. Network calibration phase

Correlation coefficients between observed and predicted values are high ($r > 0.95$, except for one partition; Table 2) and RMSEPs are satisfactorily low (0.62–1.00), meaning that down-core SSTs can be predicted within relatively low error limits. A graph showing the relationships between the observed and predicted SST_{100} in ten ANN runs is presented in Fig. 2, and summarized in Table 2. The main result of the network calibration phase is that the RMSEP estimates for SST_{100} are lower than for SST_{10} (Table 1). This confirms previous observations (Bjørklund et al., 1998), based on regressions only, on how the correlation between radiolarian-derived factor components and SST increased with depth and was optimal at about 100 m.

The reliability of our SST estimates is also confirmed by the match between the value obtained by ANN for the topmost core sample (15.5 cm, dated at 1001 years B.P.), and the observed World Ocean Atlas July–September SST (Conkright et al., 1998) at the MD95-2011 core location, i.e. the "expected" surface sediment value. The measured SST_{100} is 7.4 °C, which matches well the ANNs sediment sample SST_{100} estimate (7.1 °C).

3.2. Downcore SST_{100} predictions

The estimated mean SST_{100} and 95% confidence intervals over ten ANN runs are shown against age in Fig. 3. The results from ANN and ancillary information (depth, age, IKTF- and ANN-derived SSTs for each sample from cores HM79-4 and MD95-2011) are shown in Table 3. As the pre-Holocene evolution of our core is, in comparison to what is observed for the Holocene (see Discussion), quite typical, we will only describe it here and not discuss it in detail in the Next section, where we will instead focus on the Holocene portion.

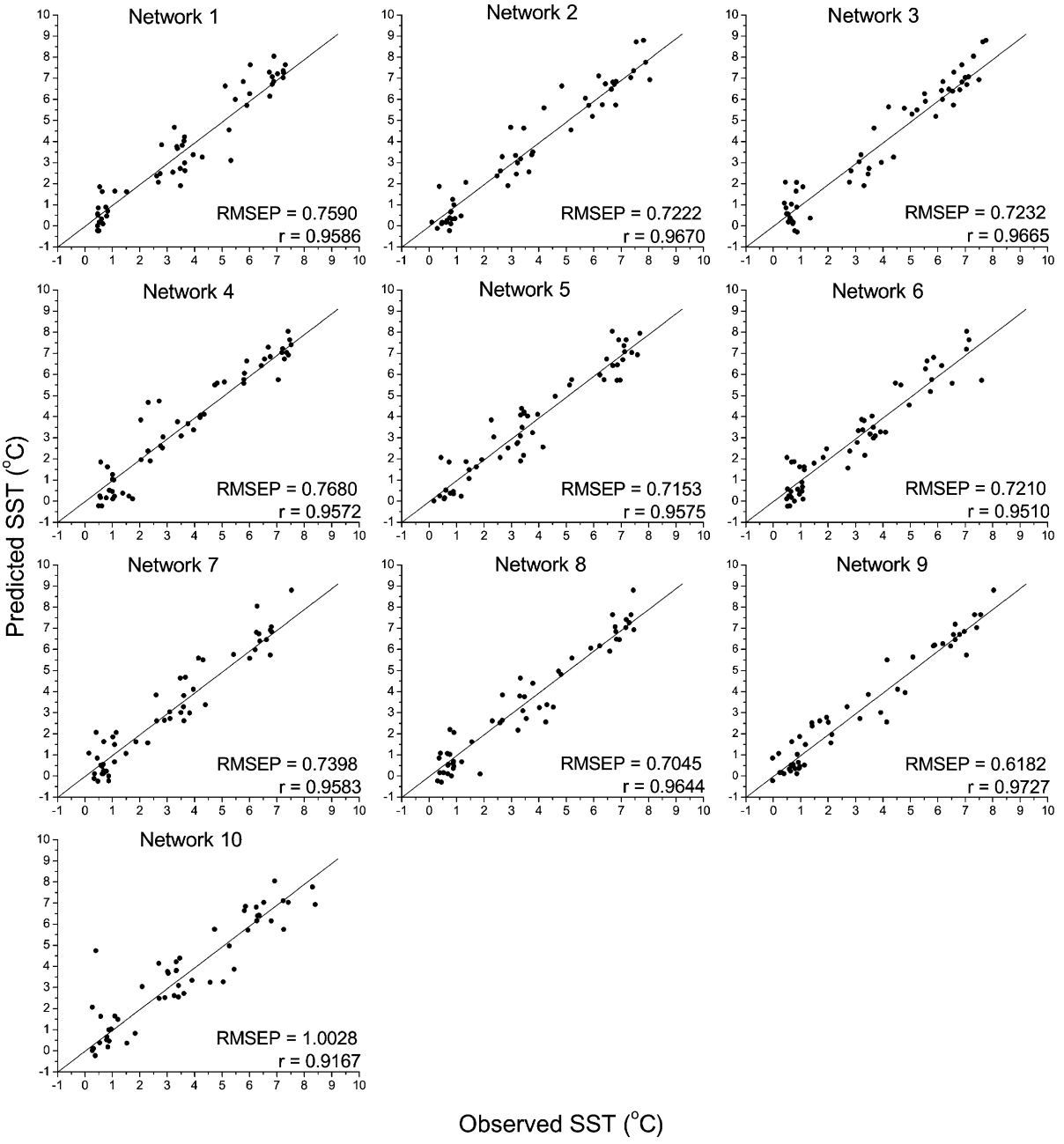

Fig. 2. Predicted vs. observed Summer Sea Temperatures (SST) for ten network runs (NGO software, 100 m water depth). RMSEPs and correlation coefficients are also reported (see also Table 2). The vertical bars represent the 95% confidence intervals based on the ten ANN runs.

The ANN paleo-SST estimates display, between 15 and 14 ka (Fig. 3), during the first half of the Bølling/Allerød, an interval with very high (over 7.5 °C) SST_{100}. Along our record, values this high are otherwise only found during the early Holocene, an interval we named the Radiolarian Holocene Optimum Temperature Interval (RHOTI). The SST_{100} then abruptly drops to ca. 0.5 °C at 13.7 ka, with a 6.2 °C cooling

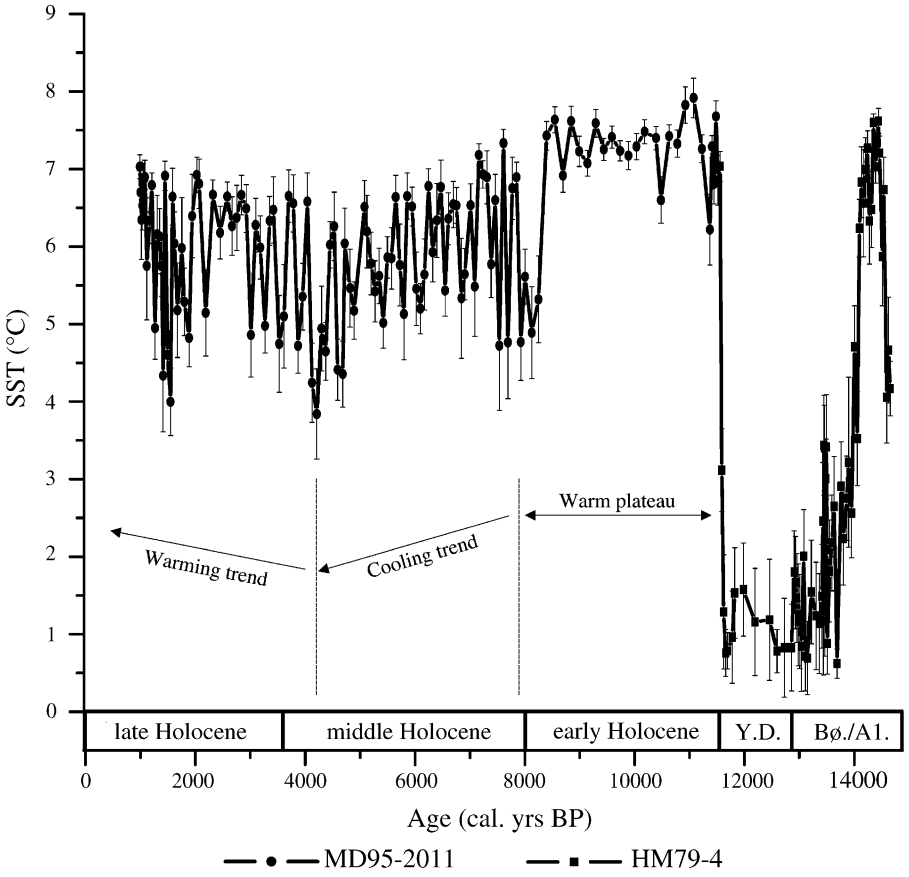

Fig. 3. SST predictions (average of ten runs) and standard deviations for cores MD95-2011 and HM79-4 (based on NGO software, 100 m water depth and setup "subset") are shown on an age scale, in calendar years Before Present. The Younger Dryas (Y.D.) and Bølling/Allerød (Bø./Al.) chronozones are after Mangerud et al. (1974). Vertical bars represent 95% confidence intervals for the ten ANN-based SST estimates. The early Holocene plateau, the middle Holocene cooling trend, and the late Holocene warming trend are also schematically indicated.

taking place in 440 years. During the time interval including the second half of the Bølling/Allerød and the Younger Dryas (13.7–11.6 ka), temperatures remain stable at low values, except for several (4–5) short-lived, centennial, warming episodes, during which temperatures rise by ca. 1 °C over the background level. The transition to the Holocene takes place over 140 years, and rapidly brings SST_{100} to early Holocene levels, i.e. around 7.5 °C. This corresponds to an average warming rate of 4.9 °C per century (6.8 °C warming over only 140 years), with rates up to more than twice as high between two consecutive samples (e.g. 11.5 °C per century between the samples dated as 11,586 and 11,552 years BP, Table 3). This local oceanic warming rate is about half the maximum rate of atmospheric temperature change during the warming at the end of the Younger Dryas, which is reported to have occurred at rates as large as 10 °C/50 years for a significant part of the Northern Hemisphere (IPCC, 2001). In comparison to recent atmospheric warming rates, however, the observed local average oceanic rate of 4.9 °C per century is quite high. In fact, model prognoses for the future, global mean, near-surface atmospheric temperature vary between 1 and 6 °C per century, with the current rate being lower than this range, at 0.1–0.2 °C/decade (IPCC, 2001).

The early Holocene (until ca. 8 ka) is characterized by relatively stable, warm conditions, with SST_{100} usually between 7 and 7.5 °C. A very rapid, almost

3 °C cooling takes place between 8.4 and 8.1 ka, and introduces an interval displaying a new style of climatic variability. In fact, after the recovery of SST_{100} to early Holocene levels at ca. 7.5 ka, the middle Holocene shows a clear trend of decreasing temperature, down to ca. 3.5 °C at 4.2 ka, with a superimposed centennial-scale variability, represented by repeated warmings and coolings of ca. 2 °C amplitude. A slightly stronger, ca. 3 °C, warming starting at 4.2 ka slightly predates the transition into the late Holocene (last 3.7 ka). Although SST_{100} still displays strong centennial variability during this interval, it follows a warming trend, with temperatures back to ca. 7 °C at 1100 years ago. The Kendall test indicates that this warming is statistically significant at the 5% level (Kendall $\tau = 0.221$), and this increase in SST_{100} since 4.2 ka is of an average order of 0.8 °C (obtained by inserting the top and bottom levels in this interval into the regression function).

The REDFIT procedure (Schulz and Mudelsee, 2002) was used to recognize cyclical patterns in the generated SST_{100} timeseries, and test the significance of peaks in the amplitude spectrum against a null-hypothesis of a red-noise background. The application of this technique to our Holocene ANN SST record (core MD95-2011) indicates the existence of a climate cycle of 278 years length. The runs test inherent in the REDFIT software indicates that the fluctuations in this timeseries are not consistent with a red-noise process (r-value = 30, which is within the 5% acceptance region of 24–41) and, as this spectral peak lies above the 98.4% false-alarm level (Thomson, 1990), the 278-year long cycle in this timeseries is statistically significant against the red-noise background.

4. Discussion

4.1. Spectral analysis of the Holocene ANN-SST record

Changes in solar activity during the Holocene have an influence over climate at millennial and centennial time scales, as it has been convincingly demonstrated for the North Atlantic (Bond et al., 1997; deMenocal et al., 2000; Bond et al., 2001). One important manifestation of solar variability is the de Vries or Suess cycle (Suess, 1965), which has an average period of 210 years, with a range of 180–220 years. This cycle has been identified in a variety of settings (Yu and Ito, 1999; Neff et al., 2001), including tree rings (Scuderi, 1993), lake sediments (Anderson, 1992), ice-core records (Raisbeck et al., 1990), and a marine sediment record from the Caribbean Sea (Nyberg et al., 2001). A ca. 200-year cyclicity has also been recognized in the high-resolution oceanic sediment record of Palmer Deep, Antarctic Peninsula, covering the last 13 ka (Domack et al., 2001). This sub-millennial variability is particularly well developed in the late Holocene and is suggested to be connected, in Palmer Deep, to cycles in productivity and Sea Surface Temperature (Leventer et al., 1996), and to solar cycles (Domack et al., 2001). Such a cycle has also been found in Lake Saki (Currie, 1995) and Pakistanian lake varves. Spectral analysis on the MD95-2011 timeseries using the REDFIT procedure (Schulz and Mudelsee, 2002), the most rigorous available for unequally sampled series, instead indicates the existence of a climate cycle of 278 years length, which is close to the de Vries or Suess cycle (Fig. 4). A significant Holocene periodicity of 230 years has been recently documented (Sarnthein et al., 2003) in a core (GeoB23258) from off the western Barents Sea shelf. This core is located along the path of the Western Spitzbergen Current (the northward extension of the Norwegian Current), and its climatic record is therefore presumably affected by most of the climatic mechanisms that are also active in our study area. Our study lends therefore support to the existence of a strong Holocene cyclicity in the Nordic Seas, with a characteristic signature for a period close to the Suess band. The recognized 278-year cyclicity is however separated from the Suess cycle, and it has also been reported (Damon and Sonett, 1989) from ^{14}C activity records, and linked to solar variability. Modelling of the solar irradiance forcing also suggests the presence of a cyclicity having a period of ca. 250 years (Weber et al., 2004). Climatic mechanisms associated to a cycle of such length are however, until today, unknown.

4.2. Downcore predictions: water column gradients?

We do not observe major differences between the ANN and IKTF methods (Fig. 5), and the remarkably lower SSTs values reconstructed by the ANNs compared to IKTF are easily accounted for, as the former

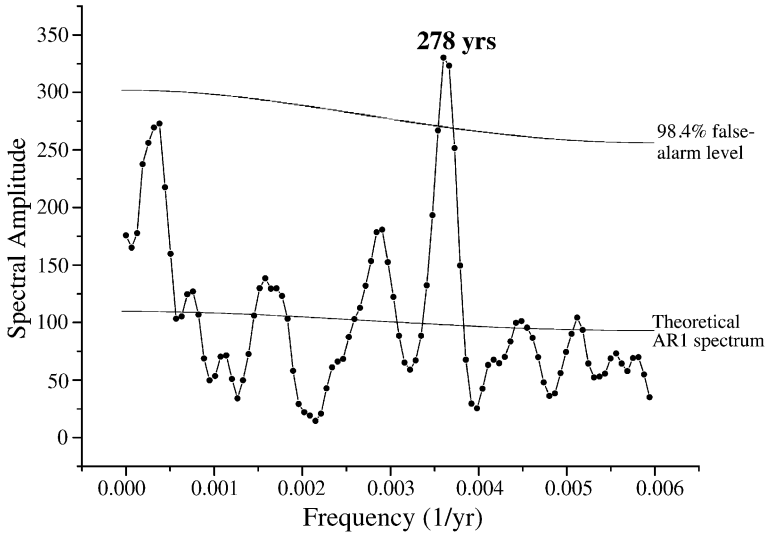

Fig. 4. Amplitude spectrum for the Holocene ANN SST record (core MD95-2011) based on the REDFIT procedure (Schulz and Mudelsee, 2002). One spectral peak at a frequency of 0.0036 above the 98.4% false-alarm level (Thomson, 1990) suggests the existence of a 278-year long cycle in this timeseries that is statistically significant against the red-noise background. The theoretical red-noise (AR [1]) spectrum is also shown.

refers to 100 m (SST_{100}), while the latter refers to 0 m water depth (SST_0). The good match in the details and in the millennial-scale variability of the two curves witnesses the reliability of both IKTF and ANN at predicting SST in the study area. The main difference consists in a slightly faster cooling in ANN SST_{100}

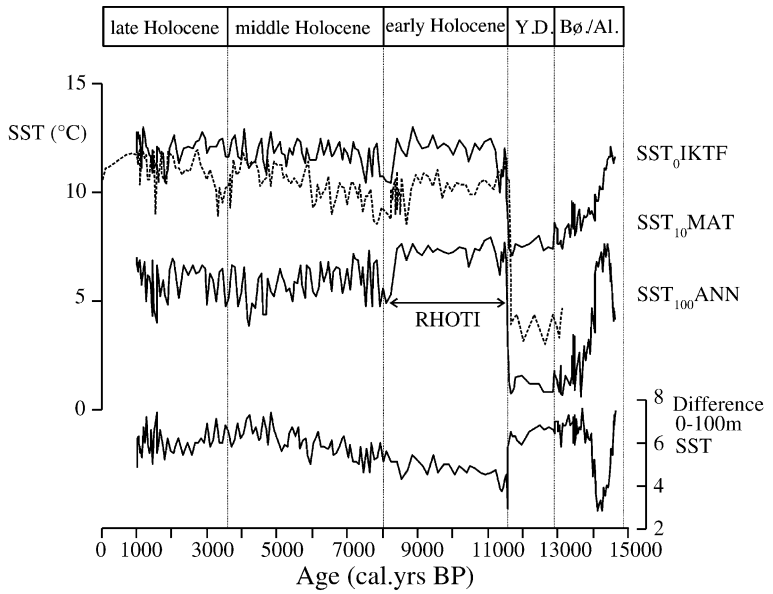

Fig. 5. Comparison between SST_{100}, reconstructed by ANN (this paper) and SST_0, reconstructed by the IKTF method (Dolven et al., 2002) for cores MD95-2011 and HM79-4. The difference between the two, representing the degree of mixing of the surface layer, is also shown, along with the Radiolarian Holocene Optimum Temperature Interval (RHOTI), roughly coinciding with the early Holocene. The chronozones are as for Fig. 3. The planktonic foraminifera MAT-derived SST_{10} (Risebrobakken et al., 2003) from core MD95-2011, on the GISP-synchronized time scale, is reported too.

compared to IKTF SST_0 from 14.3 to 13.7 ka (Fig. 5). This could represent a threshold response of the deeper mixed-layer waters to the more gradual cooling trend displayed by the shallower mixed-layer waters, or result from an artefact of the methods.

Based on the present results from ANN (SST_{100}) and previously published results for SST_0 (Dolven et al., 2002), it is possible to compare the temperature evolution from the Bølling/Allerød to present at two different levels in the water column, and to get an idea on the degree of mixing of the surface layer of the ocean (Fig. 5). A trend towards good mixing characterizes the first half of the Bølling/Allerød, while the second half of the Bølling/Allerød and the Younger Dryas are indicative of well-stratified surface layer conditions, with a ca. 7 °C SST difference between 100 and 0 m (Fig. 5). The transition to interglacial conditions in the early Holocene marks also the return to well-mixed surface waters, with a difference of only 3 °C between the two depth levels considered here. During the early and middle Holocene (until ca. 4.2 ka) one notices a trend towards progressively more stratified waters, mainly connected to the cooling of the deeper (100 m) waters, while conditions close to the surface remain relatively stable and warm. See next paragraphs for additional discussion over SST trends during the Holocene.

4.3. Comparison to other late Pleistocene–Holocene paleoclimatic records

Modern Analog Technique (MAT)-derived SSTs, based on planktonic foraminifera from the MD95-2011 core, have recently been published (Risebrobakken et al., 2003). These results are very close to our previously published SST_0 based on IKTF (Dolven et al., 2002), not indicating particularly warm SST_0 during the early Holocene, but displaying relatively stable early Holocene (11.6–8 ka) SST_0. The latter gives way to an increasing trend in SST_0 into the middle Holocene (from 8 to 4 ka), and a subsequent very slow warming trend through the late Holocene (3.6–0 ka). Our ANN-based paleo-SST_{100} results do not display the cooling trend through the Holocene that was noted in other high-latitude North Atlantic sites (Marchal et al., 2002), and in an Indian Ocean core (Naidu and Malmgren, 2005). In our record, this cooling trend is restricted to the middle Holocene. The two most obvious differences between the ANN-SSTs and MAT-SSTs concern the early Holocene and the middle Holocene, while the two datasets match quite well during the 8.2 ka cooling event. These time intervals and event will be discussed in the following sub-sections.

4.3.1. The early Holocene (11.6–8.0 ka)

In order to avoid confusion with the Holocene Climatic Optimum (HCO), taking place in the middle Holocene, from ca. 4 to 7 ka, we will refer to the early Holocene radiolarian temperatures, the highest for the Holocene, as the Radiolarian Holocene Optimum Temperature Interval (RHOTI). The presence of an early Holocene RHOTI matches the observation of a maximum in ocean surface temperature off northern Norway between ca. 10.700 and 8.900 cal. years B.P. (Hald et al., 1996), and the calculated post-glacial temperature anomalies in Greenland, which were at a maximum during the Preboreal and Boreal (Johnsen et al., 1995). This is also in accordance with stratigraphic records of the beetle *Phratora* (*Phyllodeca*) sp. cf. *P. polaris*, as this species has at present not been recorded alive in Greenland, while its fossil record shows it was widely distributed in the early Holocene and was undoubtedly favoured by the warmer climate at that time (Bennike et al., 1999). MAT-based SSTs (Risebrobakken et al., 2003) from core MD95-2011 indicate that the early Holocene may be typified by a very slight cooling trend, and its average SST is practically identical to the middle Holocene, and actually colder than the late Holocene. Optimum SSTs are recorded in other SST reconstructions for core MD95-2011, and they occur either between early and middle Holocene, at 9–7 ka, according to diatom-based IKTF (Birks and Koç, 2002), or in the middle Holocene, at 8.5–5.5 ka, as indicated by alkenones (Calvo et al., 2002). Planktic foraminifera, just as radiolarians, may be recording subsurface hydrography changes (Dolven et al., 2002; Risebrobakken et al., 2003). They are therefore imperfect recorders of shallow surface processes and conditions, compared to diatoms and nannoplankton (the latter being the producers of the alkenone signal), which live instead in very shallow water depths. Both diatoms and nannoplankton, however, are themselves affected by problems of another sort as, belonging to the sedimentary fine fraction, may be transported over

very long distances, and do not always record local SST conditions. Risebrobakken et al. (2003) argue that the lack of high SST during the early Holocene in planktic foraminifera MAT-SSTs, compared to diatom- and alkenone-based records, was caused by an eastward migration of Arctic water, forced by stronger westerlies, which influenced the subsurface water and not the uppermost sea surface water (Blindheim et al., 2000). Hald et al. (1996), however, reported on maximum ocean surface temperatures off northern Norway, based on planktonic foraminifera, during the early Holocene. This, together with the presence of a recognizable RHOTI during the early Holocene in our radiolarian ANN-derived SST_{100}, although not as clear as for diatom- and alkenone-derived SST, questions the theory of stronger westerlies during the early Holocene (Blindheim et al., 2000). These seemingly contradictory results obtained by different fossil groups should not be taken as a negative characteristic of these methods, but represent instead a very promising spinoff, as an integrated approach may be key to the estimation of the degree of water column stratification, which is a very important quantity for the validation and improvement of climate models.

In the case of the Holocene, for instance, the available evidence (HCO presence for nannoplankton, warmer early to middle Holocene for diatoms, warmer early Holocene SST_{100} for radiolarians, warmer early Holocene ocean surface temperatures for foraminifera) may also indicate a real phenomenon, i.e. a differential behavior of very shallow and subsurface waters through the different Holocene intervals. The early Holocene and the first half of the Bølling/Allerød would then represent intervals of well-mixed surface layer, with a small contrast between very shallow and 100 m depths (Fig. 5). During the middle Holocene, on the contrary, an important decoupling between these two layers would take place, and the warming would be limited to the very shallow layers, and not extend down to ca. 100 m depth. A very strong stratification of the upper water column is present during the second half of the Bølling/Allerød and the whole Younger Dryas, when SSTs are at their minimum. This is probably due to the presence of a cold, low salinity lid, which is commonly associated with the Younger Dryas cooling (Bodén et al., 1997; Spielhagen et al., 1998; Clark et al., 2001). Such a lid could actually be the cause of the Younger Dryas cooling, and model experiments (Manabe and Stouffer, 2000) suggest that the release of 0.1 Sv of freshwater over 500 years to the North Atlantic, between Greenland and Iceland, results in a drastic cooling (Younger Dryas), followed by a period, just before the Holocene warming, with very unstable ocean temperatures.

4.3.2. The 8.2 ka cooling event

This event has been recognized in many paleoclimatic records, and seems to be related to the sudden discharge into the Labrador Sea of freshwater from the periglacial Lake Agassiz (Barber et al., 1999). This localized discharge of low-density waters into very sensitive convection sites for North Atlantic Deep Water formation strongly disturbed the overturning circulation in the North Atlantic, causing its slowdown, and a consequent cooling in the areas around the North Atlantic. During this event, a reduced amount of warm Atlantic water entered the Nordic Seas, as an intermediate current, underlying the less-salty water originating from the Labrador Sea. This water stratification also probably contributed to the regional North Atlantic cooling by reducing the ocean/atmosphere heat exchange. In our ANN SST_{100} record, the 8.2 ka cooling event is clearly shown between 8.1 and 8.5 ka (Fig. 6), and represents a 2.7 °C cooling lasting 420 years. This matches quite well with that recognized in the MAT SST record, i.e. a ca. 3 °C decrease in SST centered at 8.0–8.1 ka (Risebrobakken et al., 2003). In the northern North Sea, Klitgaard-Kristensen et al. (1998) recognized that *N. pachyderma* (sin.) reaches a 15–16% abundance peak, against its background 2–7% abundance during last 10.000 cal. years B.P., and correlated this peak to the Greenland GRIP ice core 8200 years event. Knies et al. (2003) reported two prominent lows in marine organic carbon in Andfjorden that may correlate with the Preboreal Oscillation (PBO; 11.17–11.05 ka) and the Greenland 8.2 ka event, as discussed by Björck et al. (1996) and Alley et al. (1997), respectively. The PBO is probably also present in our data (Fig. 3, Table 3), showing a gradual temperature increase over three samples from 6.2 °C (11.370 cal. years B.P.) till 7.9 °C (11.074 cal. years B.P.). Klitgaard-Kristensen et al. (1998) concluded that the synchronous timing of the cooling event in the Greenland ice-cores, marine records and tree ring data from north-

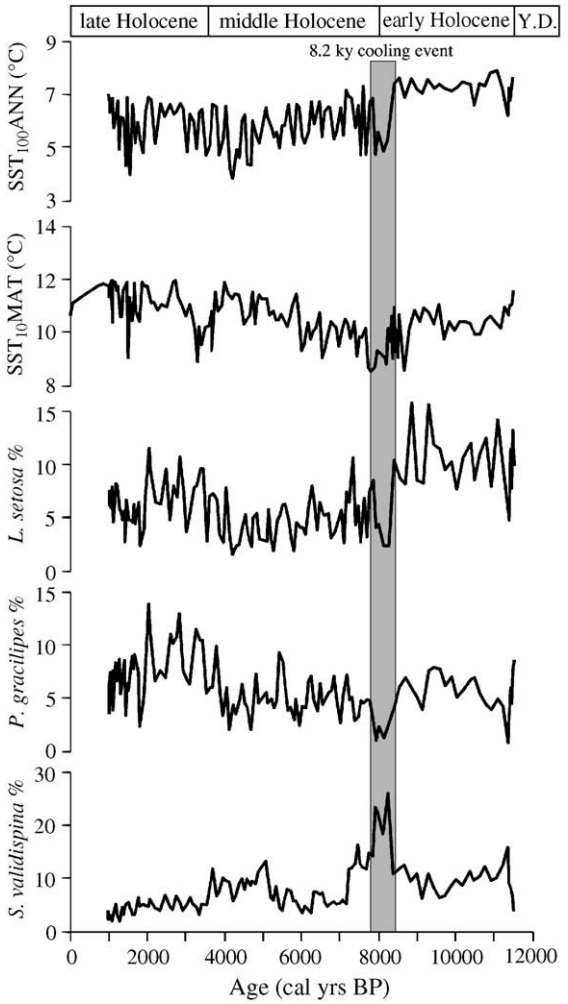

Fig. 6. Holocene changes in ANN-derived SST_{100}, and corresponding variations in the relative abundances of three radiolarian species (*L.setosa*, *P. gracilipes*, and *S. validispina*). The 8.2 ka cooling event is shaded for reference. Y.D.=Younger Dryas. The planktonic foraminifera MAT-derived SST_{10} (Risebrobakken et al., 2003) from core MD95-2011, on the GISP-synchronized time scale, is reported too.

west Europe suggests a regional influence on the North Atlantic ocean-atmosphere system and the thermohaline circulation.

The radiolarian assemblage changes associated with the 8.2 ka cooling event (Fig. 6) include a major decrease in the relative abundance of *Lithomelissa setosa* and *Pseudodictyophimus gracilipes*, while *Stylodictya validispina* displays an absolute maximum during this time interval. The first two species are main components of the warm water assemblage (Factor 4) recognized in the study area (Cortese et al., 2003). Their modern distribution is either very strongly linked to the warm Norwegian Current (*L. setosa*), or centered around the eastern boundary of the Arctic Front (*P. gracilipes*), in the gyre east of Jan Mayen/Iceland Plateau, i.e. they are found in waters warmer than those present today on the Iceland Plateau (Cortese et al., 2003). According to their modern distribution, it seems that the radiolarian assemblage change during the 8.2 ka event was represented rather by a decrease in warm water species, than by an increase in cold ones. This may indicate a reduction of the importance of the warm Norwegian Current in the study area, a consequence of the slowdown of the North Atlantic overturning circulation. The latter is, as mentioned earlier, a result of freshwater discharges from periglacial lakes around the Laurentide ice sheet, the current explanation for the 8.2 ka cooling (Barber et al., 1999; Alley et al., 1997). The shift in abundance of *S. validispina* (from 11% to 26%, Fig. 6) may also be a response to this meltwater flux, as closely related representatives of the family Spongodiscidae, i.e. *Spongotrochus glacialis*, *Spongaster tetras*, *Stylochlamydium venustum* have been demonstrated (Boltovskoy, 1998; Nimmergut and Abelmann, 2002) to live in the shallowest part of the water column, and to be able to adapt to a broad range of temperature and salinity conditions. In the Sea of Okhotsk, for example, sea ice melt has a strong impact, and a low-salinity layer develops at the surface during the spring–summer melt season. In the Sea of Okhotsk, juvenile Spongodiscidae display an abundance peak in the surface layer (Nimmergut and Abelmann, 2002), and are almost the only radiolarians capable of thriving in such low salinity conditions. Blueford (1983) also demonstrated that juvenile and adult Spongodiscidae were dominant in the surface sediments of the shallow northeastern parts of the Bering Sea, an area also influenced by low salinity conditions.

4.3.3. The middle (8.0–3.6 ka) and late (3.6–0 ka) Holocene

The SST reconstructions for the 8–3.6 ka interval, roughly corresponding to the middle Holocene, are substantially different between ANN SST_{100} (showing a cooling trend) and MAT SST, indicating a warming

trend (Risebrobakken et al., 2003). The latter, however, is difficult to reconcile with the abundances of *N. pachyderma* sinistral morphotype during the middle Holocene, which should be indicative of a relatively constant, or even slightly cooling trend. The presence of a cooling trend is also supported by the maximum values reached by *Globigerina quinqueloba* during the middle Holocene, indicative of repeated Arctic water influence into the Norwegian Sea at this time, as this species is associated with the Arctic Front area (Johannessen et al., 1994). However, the general Holocene trends of ANN SST_{100} and MAT SSTs are relatively well comparable. There is an apparent discrepancy between the two methods for the absolute SST values (4–5 °C difference during the Holocene, 2 °C difference during the Younger Dryas, with MAT recording, for both time intervals, warmer temperatures). This is, however, easily accounted for, as it relates to the different water depth the reconstructed SSTs refer to: 100 m depth for ANN (this paper), 10 m depth for MAT (Risebrobakken et al., 2003). In our MD95-2011 record, the late Holocene is characterized by a slight, but statistically significant, warming trend, with ANN SST_{100} recovering after the middle Holocene cooling trend. A slight trend towards a less-stratified surface layer is also evident during the late Holocene (Fig. 5), after the maximum Holocene mixed-layer stratification, which was reached during the youngest portion of the middle Holocene.

5. Summary

The main aim of this study was to apply Artificial Neural Networks to the reconstruction of surface water temperature in an area that is very sensible to heat transport to high latitudes and to thermohaline overturning. The main results of this study can be so summarized:

- ANN have been successfully calibrated in the Nordic Seas, with both high correlation coefficients between observed and predicted values ($r > 0.95$, but for one case) and satisfactorily low RMSEPs (0.62–1.00 °C), which allows the reconstruction of past SSTs within relatively low error limits;
- Optimal correlation is found for the summer temperature at 100 m depth, indicating how this season and depth are particularly important for the formation of the radiolarian assemblage signal in the study area at present;
- The first half of the Bølling/Allerød and the early Holocene represent time intervals when SST_{100} reached a maximum;
- The Preboreal Oscillation (PBO) and the Greenland 8.2 ka event are both present in our record. There is a drop of 1.7 °C and a rise of 1.1 °C in and out of the PBO, respectively, while the 8.2 ka event is represented by a 2.7 °C cooling lasting 420 years;
- The middle Holocene is characterized by a cooling trend in SST_{100}, while the late Holocene displays a warming trend;
- The Holocene SST_{100} signal includes a strong cyclicity (278 years period) close to the Suess band;
- There is good agreement between the ANN and IKTF-derived SSTs: the main difference is represented by a faster cooling in ANN SST_{100} compared to IKTF SST_0 during the Bølling/Allerød;
- MAT-derived SSTs based on planktonic foraminifera also match well our reconstructions, with the exception of the absence of a SST optimum during the early Holocene, and a warming trend during the middle Holocene;
- The highest SSTs during the Holocene occur at different times and depths according to different methods and fossil groups (*underlined*=our data, evidence from other methods cited in the Discussion paragraph): early Holocene (*SST_{100}*, *radiolarians*, *ANN*), between early and middle Holocene (SST_0, diatoms, IKTF), middle Holocene (SST_0, alkenones). Other methods do not indicate the presence of a clear SST optimum during the Holocene (SST_{10}, planktonic foraminifera, MAT; *SST_0*, *radiolarians*, *IKTF*). This information can be used to reconstruct the degree of mixing of the upper water column.

Acknowledgements

Dave Lazarus and an anonymous reviewer are thanked for their suggestions and improvements to the manuscript. We warmly thank Øyvind Hammer for reading and commenting an earlier version of the manuscript, which was revised according to his

remarks. Sincere thanks go to Björg Risebrobakken who generously shared her data. G. Cortese was supported, during the realization of this paper, by the Deutsche Forschungsgemeinschaft as part of the DFG-Research Center "Ocean Margins" of the University of Bremen, No. RCOM0288. The University of Oslo and the Norwegian Research Council funded J.K. Dolven when producing the radiolarian data from HM79-4 and MD95-2011.

References

Abelmann, A., Brathauer, U., Gersonde, R., Sieger, R., Zielinski, U., 1999. Radiolarian-based transfer function for the estimation of sea surface temperatures in the Southern Ocean (Atlantic sector). Paleoceanography 14 (3), 410–421.

Alley, R.B., Mayewski, P.A., Sowers, T., Stuiver, M., Taylor, K.C., Clark, P.U., 1997. Holocene climatic instability: a prominent widespread event 8200 years ago. Geology 25, 483–486.

Anderson, R.Y., 1992. Possible connections between surface winds, solar activity, and the earth's magnetic field. Nature 358, 51–53.

Barber, D.C., Dyke, A., Hillaire-Marcel, C., Jennings, A.E., Andrews, J.T., Kerwin, M.W., Bilodeau, G., McNeely, R., Southon, J., Morehead, M.D., Gagnonk, J.-M., 1999. Forcing of the cold event of 8200 years ago by catastrophic drainage of Laurentide lakes. Nature 400, 344–348.

Bennike, O., Björck, S., Böcher, J., Hansen, L., Heinemeier, J., Wohlfahrt, B., 1999. Early Holocene plant and animal remains from North-East Greenland. Journal of Biogeography 26, 667–677.

Birks, H.J.B., 1995. Quantitative palaeoenvironmental reconstructions. In: Maddy, D., Brew, J.S. (Eds.), Statistical Modeling of Quaternary Science Data. Quaternary Research Association, Cambridge, U.K., pp. 161–254.

Birks, H.H., Gulliksen, S., Haflidason, H., Mangerud, J., 1996. New radiocarbon dates for the Vedde Ash and the Saksunarvatn Ash from western Norway. Quaternary Research 45, 119–127.

Birks, C.J.A., Koç, N., 2002. A high-resolution diatom record of late-Quaternary sea-surface temperatures and oceanographic conditions from the eastern Norwegian Sea. Boreas 31, 323–344.

Björck, S., Kromer, B., Johnson, S., Bennike, O., Hammarlund, D., Lemdahl, G., Possnert, G., Rasmussen, T.L., Wohlfahrt, B., Hammer, C.U., Spurk, M., 1996. Synchronized terrestrial–atmospheric deglacial records around the North Atlantic. Science 274, 1155–1160.

Bjørklund, K.R., 1974. The seasonal occurrence and depth zonation of radiolarians in Korsfjorden, Western Norway. Sarsia 56, 13–42.

Bjørklund, K.R., Cortese, G., Swanberg, N., Schrader, H.J., 1998. Radiolarian faunal provinces in surface sediments of the Greenland, Iceland and Norwegian (GIN) Seas. Marine Micropaleontology 35, 105–140.

Blindheim, J., Borokov, V., Hansen, B., Malmberg, S.A., Turrell, W.R., Østerhus, S., 2000. Upper layer cooling and freshening in the Norwegian Sea in relation to atmospheric forcing. Deep Sea Research, Part I 47, 655–680.

Blueford, J.R., 1983. Distribution of Quaternary radiolaria in the Navarin Basin geologic province, Bering Sea. Deep-Sea Research 30 (7A), 763–781.

Bodén, P., Fairbanks, R.D., Wright, J.D., Burckle, L.H., 1997. High-resolution stable isotope records from southwest Sweden: the drainage of the Baltic Ice Lake and Younger Dryas ice margin oscillations. Paleoceanography 12, 39–49.

Boltovskoy, D., 1998. Classification and distribution of South Atlantic recent polycystine radiolaria. Paleontologica Electronica 1 (2).

Bond, G., Showers, W., Cheseby, M., Almasi, P., deMenocal, P., Priore, P., Hajdas, I., Bonani, G., 1997. A pervasive millennial-scale cycle in North Atlantic Holocene and glacial climates. Science 278, 1257–1266.

Bond, G., Kromer, B., Beer, J., Muscheler, R., Evans, M.N., Showers, W., Hoffmann, S., Lotti-Bond, R., Hajdas, I., Bonani, G., 2001. Persistent solar influence on North Atlantic climate during the Holocene. Science 294, 2130–2136.

Calvo, E., Grimalt, J., Jansen, E., 2002. High resolution U^{K}_{37} sea surface temperature reconstruction in the Norwegian Sea during the Holocene. Quaternary Science Reviews 21, 1385–1394.

Clark, P.U., Marshall, S.J., Clarke, G.K.C., Hostetler, S., Licciardi, J.M., Teller, J.T., 2001. Freshwater forcing of abrupt climate change during the last glaciation. Science 293, 283–287.

Conkright, M., Levitus, S., O'Brien, T., Boyer, T., Antonov, J., Stephens, C., 1998. World Ocean Atlas 1998 CD-ROM Data Set Documentation, National Oceanographic Data Center (NODC) Internal Report, Silver Spring, Maryland.

Cortese, G., Abelmann, A., 2002. Radiolarian-based paleotemperatures during the last 160 kyrs at ODP Site 1089 (Southern Ocean, Atlantic Sector). Palaeogeography, Palaeoclimatology, Palaeoecology 182 (3–4), 259–286.

Cortese, G., Bjørklund, K.R., Dolven, J.K., 2003. Polycystine radiolarians in the Greenland–Iceland–Norwegian Seas: species and assemblage distribution. Sarsia 88, 65–88.

Currie, R.G., 1995. Luni-solar and solar cycle signals in Lake Saki varves and further experiments. International Journal of Climatology 15 (8), 893.

Damon, P.E., Sonett, C.P., 1989. Solar and terrestrial components of the atmospheric ^{14}C variation spectrum. In: Sonett, C.P. (Ed.), The Sun in Time. Univ. Arizona Press, Tucson, AZ.

deMenocal, P., Ortiz, J., Guilderson, T., Sarnthein, M., 2000. Coherent high- and low-latitude climate variability during the Holocene warm period. Science 288, 2198–2202.

Dolven, J.K., Bjørklund, K.R., 2001. An early Holocene peak occurrence and recent distribution of *Rhizoplegma boreale* (Radiolaria): a biomarker in the Norwegian Sea. Marine Micropaleontology 42, 25–44.

Dolven, J.K., Cortese, G., Bjørklund, K.R., 2002. A high-resolution radiolarian-derived paleotemperature record for the Late Pleistocene–Holocene in the Norwegian Sea. Paleoceanography 17 (4), 1072. doi:10.1029/2002PA000780.

Domack, E., Leventer, A., Dunbar, R., Taylor, F., Brachfeld, S., Sjunneskog, C., ODP Leg 178 Scientific Party, 2001. Chronology of the Palmer Deep site, Antarctic Peninsula: a Holocene palaeoenvironmental reference for the circum-Antarctic. The Holocene 11, 1–9.

Ganopolski, A., Rahmstorf, S., 2001. Rapid changes of glacial climate simulated in a coupled climate model. Nature 409, 153–158.

Hald, M., Dokken, T., Hagen, S., 1996. Paleoceanography on the European Arctic Margin during the last deglaciation. In: Andrews, J.T., Austin, W.E.N., Bergsten, H., Jennings, A.E., et al., (Eds.), The Quaternary Paleoceanography of the North Atlantic Margins, 111. Geological Society Special Publication, pp. 275–287.

Hutson, W.H., 1979. The Agulhas Current during the late Pleistocene: analysis of modern faunal analogs. Science 207, 64–66.

Imbrie, J., Kipp, N.G., 1971. A new micropaleontological method for quantitative paleoclimatology: application to a late Pleistocene Caribbean core. In: Turekian, K. (Ed.), Late Cenozoic Glacial Ages. Yale University Press, New Haven, Connecticut, pp. 71–181.

IPCC, 2001. Climate change 2001: the scientific basis. Contribution of Working Group I to the Third Assessment Report of the Intergovernmental Panel on Climate Change. Cambridge University Press, Cambridge, United Kingdom. 881 pp.

Johannessen, T., Jansen, E., Flatøy, A., Ravelo, A.C., 1994. The relationship between surface water masses, oceanographic fronts and paleoclimatic proxies in surface sediments of the Greenland, Iceland and Norwegian Seas. In: Zahn, R., Kaminski, M., Labeyrie, L. (Eds.), Carbon Cycling in Glacial Ocean: Constraints on the Ocean's Role in Global Change, NATO ASI Series. Springer-Verlag, New York, pp. 61–85.

Johnsen, S.J., Dahl-Jensen, D., Dansgaard, W., Gundestrup, N., 1995. Greenland palaeotemperatures derived from GRIP bore hole temperature and ice core isotope profiles. Tellus 47B, 624–629.

Kendall, M., Ord, J.K., 1990. Time Series, 3rd ed. Edward Arnold. 296 pp.

Klitgaard-Kristensen, D., Sejrup, H.P., Haflidason, H., Johnsen, S., Spurk, M., 1998. A regional 8200 cal. yr BP cooling event in northwest Europe, induced by final stages of the Laurentide ice-sheet deglaciation? Journal of Quaternary Science 13 (2), 165–169.

Knies, J., Hald, M., Ebbesen, H., Mann, U., Vogt, C., 2003. A deglacial—middle Holocene record of biogenous sedimentation and paleoproductivity changes from the northern Norwegian shelf. Paleoceanography 18 (4), 1096. doi:10.1029/2002PA000872.

Koc-Karpuz, N., Jansen, E., 1992. A high-resolution diatom record of the last deglaciation from the SE Norwegian Sea: documentation of rapid climatic changes. Paleoceanography 7, 499–520.

Leventer, A., Domack, E.W., Ishman, E., Brachfeld, S., McClennen, C.E., Manley, P., 1996. Productivity cycles of 200–300 years in the Antarctic Peninsula region: understanding linkages among the sun, atmosphere, oceans, sea ice, and biota. Geological Society of America Bulletin 108, 1626–1644.

Malmgren, B.A., Nordlund, U., 1997. Application of artificial neural networks to paleoceanographic data. Palaeogeography, Palaeoclimatology, Palaeoecology 136, 359–373.

Manabe, S., Stouffer, R.J., 2000. Study of abrupt climate change by a coupled ocean–atmosphere model. Quaternary Science Reviews 19, 285–299.

Mangerud, J., Anderson, S.T., Berglund, B.E., Donner, J., 1974. Quaternary stratigraphy of Norden, a proposal for terminology and classification. Boreas 3, 109–128.

Marchal, O., Cacho, I., Stocker, T.F., Grimalt, J.O., Calvo, E., Martrat, B., Shackleton, N., Vautravers, M., Cortijo, E., van Kreveld, S., Andersson, C., Koç, N., Chapman, M., Sbaffi, L., Duplessy, J.C., Sarnthein, M., Turon, J.L., Duprat, J., Jansen, E., 2002. Apparent long-term cooling of the sea surface in the northeast Atlantic and Mediterranean during the Holocene. Quaternary Science Reviews 21, 455–483.

McCulloch, W.S., Pitts, W., 1943. A logical calculus of the idea immanent in nervous activity. Bulletin of Mathematical Biophysics 5, 115–133.

Molina-Cruz, A., 1984. The radiolarian remains as indicators of upwelling processes: the Peruvian connection. Marine Micropaleontology 9, 53–75.

Moore Jr., T.C., 1973. Late Pleistocene–Holocene oceanographic changes in the northeastern Pacific. Quaternary Research 3 (1), 99–109.

Morley, J.J., 1979. A transfer function for estimating paleoceanographic conditions, based on deep-sea surface distribution of radiolarian assemblages in the South Atlantic. Quaternary Research 12, 381–395.

Naidu, P.D., Malmgren, B.A., 2005. Seasonal Sea Surface Temperature contrast between Holocene and Last Glacial Maximum in the Arabian Sea: modulated by monsoon upwelling. Paleoceanography 20, PA1004. doi:10.1029/2004PA001078.

Neff, U., Burns, S.J., Mangini, A., Mudelsee, M., Fleitmann, D., Matter, A., 2001. Strong coherence between solar variability and the monsoon in Oman between 9 and 6 kyr ago. Nature 411, 290–293.

Nimmergut, A., Abelmann, A., 2002. Spatial and seasonal changes of radiolarian standing stocks in the Sea of Okhotsk. Deep-Sea Research I 49, 463–493.

Nyberg, J., Kuijpers, A., Malmgren, B.A., Kunzendorf, H., 2001. Late Holocene changes in precipitation and hydrography recorded in marine sediments from the northeastern Caribbean Sea. Quaternary Research 56, 87–102.

Pflaumann, U., Duprat, J., Pujol, C., Labeyrie, L., 1996. SIMMAX: a modern analog technique to deduce Atlantic sea surface temperatures from planktonic foraminifera in deep-sea sediments. Paleoceanography 11, 15–35.

Pisias, N.G., Roelofs, A., Weber, M., 1997. Radiolarian-based transfer functions for estimating mean surface ocean temperatures and seasonal range. Paleoceanography 12 (3), 365–379.

Raisbeck, G.M., Yiou, F., Jouzel, J., Petit, J.R., 1990. ^{10}Be and ^{2}H in polar ice cores as a probe of the solar variability's influence on climate. Philosophical Transactions of the Royal Society of London. A 330, 463–470.

Risebrobakken, B., Jansen, E., Andersson, C., Mjelde, E., Hevrøy, K., 2003. A high-resolution study of Holocene paleoclimatic

and paleoceanographic changes in the Nordic Seas. Paleoceanography 18 (1), 1017. doi:10.1029/2002PA000764.

Sarnthein, M., Van Kreveld, S., Erlenkeuser, H., Grootes, P.M., Kucera, M., Pflaumann, U., Schulz, M., 2003. Centennial-to-millennial-scale periodicities of Holocene climate and sediment injections off the western Barents shelf, 75 degrees N. Boreas 32 (3), 447–461.

Schlitzer, R., 2000. Ocean Data View. http://www.awi-bremerhaven.de/GEO/ODV.

Schröder-Ritzrau, A., 1995. Aktuopaläontologische Untersuchung zu Verbreitung und Vertikalfluss von Radiolarien sowie ihre räumliche und zeitliche Entwicklung im Europäischen Nordmeer. Ph.D. Thesis, Universität zu Kiel.

Schulz, M., Mudelsee, M., 2002. REDFIT: estimating red-noise spectra directly from unevenly spaced paleoclimatic time series. Computers and Geosciences 28, 421–426.

Scuderi, L.A., 1993. A 2000-year tree ring record of annual temperatures in the Sierra Nevada Mountains. Science 259, 1433–1436.

Spielhagen, R.F., Nørgaard-Pedersen, N., Erlenkauser, H., Grootes, P.M., Heinemeier, J., 1998. A meltwater event in the Arctic Ocean before the Younger Dryas. Paper presented at the 6th International Conference on Paleoceanography, UNESCO, Lisbon, 23-28 August.

Suess, H.E., 1965. Secular variations of the cosmic-ray-produced Carbon-14 in the atmosphere and their interpretation. Journal of Geophysical Research 70, 5937–5952.

ter Braak, C.J.F., 1986. Canonical correspondence analysis: a new eigenvector technique for multivariate direct gradient analysis. Ecology 67, 1167–1179.

ter Braak, C.J.F., Juggins, S., 1993. Weighted averaging partial least squares regression (WA-PLS): an improved method for reconstructing environmental variables from species assemblages. Hydrobiologia 269–270, 485–502.

Thomson, D.J., 1990. Time series analysis of Holocene climate data. Philosophical Transactions of the Royal Society of London. Series A 330, 601–616.

Waelbroeck, C., Labeyrie, L.D., Duplessy, J.C., Guiot, J., Labracherie, M., Leclaire, H., Duprat, J., 1998. Improving past sea surface temperature estimates based on planktonic fossil faunas. Paleoceanography 13 (3), 272–283.

Weber, S.L., Crowley, T.J., van der Schrier, G., 2004. Solar irradiance forcing of centennial climate variability during the Holocene. Climate Dynamics 22 (5), 539–553.

Yu, Z., Ito, E., 1999. Possible solar forcing of century-scale drought frequency in the northern Great Plains. Geology 27, 263–266.